COO-2781-6TR

ACOUSTIC CAVITATION AS A MECHANISM OF FRAGMENTATION OF HOT MOLTEN DROPLETS IN COOL LIQUIDS

by

M. Kazimi
C. Watson
D. Lanning
W. Rohsenow
N. Todreas

November 1976

Department of Nuclear Engineering
Massachusetts Institute of Technology
77 Massachusetts Avenue
Cambridge, Massachusetts 02139

Approved November 1976

Neil E. Todreas
Principal Investigator

DISCLAIMER

THIS PAGE

WAS INTENTIONALLY

LEFT BLANK

Reports and Papers Published Under

MIT Fuel-Coolant Interaction Project

(This project was funded until June 30, 1975 by ANL and reports issued as 31-109-38-2831-XX; Starting July 1, 1975 reports were issued as COO-2781-XX).

Progress Reports (Available from National Technical Information Service, U.S. Department of Commerce, Springfield, Va. 22151

W.F. Lenz, G. Shiralker and N. Todreas, Fuel Coolant Thermal Interaction Project UC 79P, COO-2781-1, Nov. 1975.

W.F. Lenz, G. Shiralker and N. Todreas, Fuel Coolant Thermal Interaction Project UC 79P, COO-2781-2, Feb. 1976.

G. Shiralker, W.F. Lenz and M. Corradini, Fuel Coolant Thermal Interaction Project UC 79P, COO-2781-3, April 1976

G. Shiralker, W.F. Lenz and M. Corradini, Fuel Coolant Thermal Interaction Project UC 79P, COO-2781-5, Oct. 1976.

Topical Reports (Available from National Technical Information Service, U.S. Department of Commerce, Springfield, Va. 22151)

Mujid S. Kazimi, "Theoretical Studies on Some Aspects of Molten Fuel-Coolant Thermal Interaction," 31-109-38-2831-1 TR, MITNE-155, May 1973.

Charles E. Watson, "Transient Heat Transfer Induced Pressure Fluctuations in the Fuel-Coolant Interaction," 31-109-38-2831-2 TR, MITNE-156, August 1973.

Trond A. Bjornard, "An Experimental Investigation of Acoustic Cavitation as a Fragmentation Mechanism of Molten Tin Droplets in Water," 31-109-38-2831-3 TR, MITNE-163, May 1974.

Glen Bjorkquist, "An Experimental Investigation of the Fragmentation of Molten Metals in Water," 31-109-38-2831-4 TR June 1975.

Roland B. Knapp, "Thermal Stress Initiated Fracture as a Fragmentation Mechanism in the UO_2-Sodium Fuel-Coolant Interaction," 31-109-38-2831-5 TR, May 1975.

Topical Reports (Continued)

Michael Corradini, "Prediction of Minimum UO_2 Particle Size Based on Thermal Stress Initiated Fracture Model," COO-2781-4 TR, August 1976.

M. Kazimi, C. Watson, D. Lanning W. Rohsenow & N. Todreas, "Acoustic Cavitation as a Mechanism of Fragmentation of Hot Molten Droplets in Cool Liquids," COO-2781-6 TR, November 1976.

G.S. Shiralkar, "An Investigation of the Fragmentation of Molten Metals Dropped into Cold Water," COO-2781-7 TR, November 1976.

Papers and Summaries

M.S. Kazimi, N.E. Todreas, D.D. Lanning and W.M. Rohsenow "A Criterion for Free-Contact Fragmentation of Hot Molten Materials in Coolants," Transactions of the American Nuclear Society, Vol. 5, No. 2, p. 835, November 1972.

M.S. Kazimi, N.E. Todreas, W.M. Rohsenow and D.D. Lanning "A Theoretical Study of the Dynamic Growth of a Vapor Film Around a Hot Sphere in a Coolant," Fifth International Heat Transfer Conference, Tokyo, 1974.

T.A. Bjornard, W.M. Rohsenow and N. E. Todreas, "The Pressure Behavior Accompanying the Fragmentation of Tin in Water," American Nuclear Society Transactions, Vol. 19, pp. 247-249, 1974.

R. Knapp and N. Todreas, "Thermal Stress Initiated Fracture as a Fragmentation Mechanism in the UO_2-Sodium Fuel-Coolant Interaction," Nuclear Engineering and Design 35, pp. 69-85, (1975).

Associated in part with this contract -- G.J. Vaughan, L. Caldarola, N.E. Todreas, "A Model for Fuel Fragmentation During Molten Fuel/Coolant Thermal Interactions," International Meeting on Fast Reactor Safety and Related Physics Chicago, 6-8 October 1976.

PREFACE

In reviews of fragmentation hypotheses, the acoustic cavitation hypothesis is generally included with reference made to Kazimi's thesis [34]. While the hypothesis was initially proposed there, extensive development of the pressure interaction between the vapor film and the drop was carried out by Charles Watson [45] to complete the mathematical description of this model. This report draws together both efforts to present a comprehensive description of the model.

Since the report was first written, it has been receiving extensive comment from within and outside M.I.T., principally based on our own experiments and energy balance estimates. A supplement is added to this report to present these comments and our ideas on approaches to resolve the inconsistencies identified. While it is demonstrated that each comment may possibly be resolved by relaxation of original assumptions, the net result would be a more complex hypothesis.

Therefore at this time we prefer to develop and examine other hypotheses for the fragmentation mechanism. This report is issued at this time to record the complete acoustic cavitation hypothesis for other investigators and for possible further reference in our own efforts.

ABSTRACT

A mechanism that explains several of the observations of fragmentation of hot molten drops in coolants is presented. The mechanism relates the fragmentation to the development of acoustic cavitation and subsequent bubble growth within the molten material. The cavitation is assumed due to the severe pressure excursions calculated within the hot material as a result of the pressure pulses accompanying coolant vaporization at the sphere surface. The growth of the cavitation vapor nuclei inside the hot drop is shown to be influenced by the subsequent long duration surface pressure pulses. The variation of the amplitude of these surface pulses with experimental variables is shown to exhibit the same trends with these variables as does the variation in extent of fragmentation.

TABLE OF CONTENTS

TABLE OF CONTENTS (Continued)

1. INTRODUCTION

Fragmentation of molten UO_2 as it contacts sodium has been observed in transient fuel pin metldown experiments in the TREAT reactor [1] as well as in small scale laboratory experiments [2,3]. The creation of a large heat transfer area due to fragmentation of molten fuel contacting sodium under LMFBR accident conditions may theoretically lead to generation of high pressures and potentially damaging mechanical work [4,5]. An accurate assessment of the consequences of direct contract of molten fuel and sodium requires an understanding of the physical mechanisms leading to the dispersion of the molten fuel and the influence of the conditions of contact of the fluids on the dispersion process.

Fragmentation of hot molten materials as they contact liquids has been observed under four distinguishable contact conditions. Entrapment Fragmentation of the hot liquid is induced by the evaporation of coolant entrapped between the hot molten material and a solid surface. The experiments of Long [6] involving dropping of large quantities (~50 lbs) of molten aluminum in water could be evidence of entrapment. Impact Fragmentation was demonstrated in the shock tube experiments of Wright [7] and Darby [8]. In these experiments a water column held in a tube impacted on hot molten metals resulting in fragmentation of the metals. Hydrodynamic Fragmentation has been demonstrated in the experiments of

Ivins [9] and Delhaye [10] involving the fragmentation of mercury in water under isothermal conditions. This mode of fragmentation is caused by the nonuniformity of the forces resisting the motion of a deformable body in a fluid. Hydrodynamic fragmentation has been long recognized and utilized in atomization of chemical fuels. An excellent review of hydrodynamic fragmentation has been given by Hinze [11].

A fourth mode of fragmentation has been demonstrated in several experiments involving the dropping of small amounts (of the order of one gram) of hot molten materials into relatively cold liquid pools. The observed fragmentation occurred under conditions that do not lead to fragmentation by the preceding three modes (away from solid surfaces, in the absence of impact conditions and at relative velocities between the two fluids below that required for hydrodynamic fragmentation). This mode of fragmentation, which we call Free-Contact Fragmentation, is highly influenced by the temperatures of the two fluids. This indicates the thermal nature of the mechanism inducing this mode of fragmentation. The purpose of this paper is to propose a mechanism for inducing this mode of fragmentation based on the development of acoustic cavitation and subsequent bubble growth within the hot molten materials and to examine the validity of this mechanism in light of the available experimental observations. The role of the pressure oscillations within the vapor film

generated at the surface of the hot molten material as it is dropped into a cool pool is investigated as the means for ultimately actuating acoustic cavitation.

2. SUMMARY OF THE EXPERIMENTAL OBSERVATIONS OF FREE-CONTACT FRAGMENTATION

The fragmentation of hot molten materials in the form of small drops as they contact relatively cold liquids has been observed at several laboratories. The effects of the material and temperature of both the hot drop and the coolant on the fragmentation behavior have usually been the subject of these experimental studies. The most commonly used materials in such experiments have been molten metals as hot drops and water as the coolant pool. A limited number of experiments using molten uranium dioxide dropped into sodium have also been reported by Amblard [2] and Armstrong [3]. The essential findings of these experimental studies are summarized below.

2.1 Hot Drop Material. Fragmentation occurs for some but not all hot molten materials dropped with equal initial temperatures in water. This was first demonstrated by Swift and Pavlik [12], and then confirmed by Witte et al [13] and Cho [14]. Representative data are shown in Figure 1.

2.2 Coolant Pool Temperature. For various tested materials, fragmentation in water is reduced as water temperature is

increased [12-15,17]. Figure 2a illustrates this effect for tin and bismuth. McCracken's [16] data generally support this behavior except that the extent of fragmentation decreased sharply over a narrow range with increasing temperature and somewhat of a decrease in fragmentation was observed at temperatures below this narrow range. However, fragmentation of stainless steel in highly subcooled sodium (200-400°C) is enhanced by the increase in the sodium temperature. Qualitative results of Swift and Pavlik [12] indicate this trend is continued up to a sodium temperature of 820°C. Armstrong's quantitative results [3] as shown in Figure 3a indicate a reversal of such a trend as the sodium temperature is increased between 400-600°C.

2.3 Initial Hot Drop Temperature. In most experiments the increase in the initial drop temperature leads to an increase in the extent of fragmentation [14,16] as shown in Fig. 4a. However, in Cho's experiments of dropping molten tin in water [17], the fragmentation of tin diminished as the tin temperature increased above 550°C. This may be attributable to the limited pool depth used in these experiments, and hence to the fact that tin was not in an infinite coolant pool throughout the interaction.

2.4 Drop Radius. Limited data from experiments by Witte [12] and Cho [17] are available with which to discern trends of fragmentation with drop radius. By averaging the results

of individual runs reportedly conducted at identical conditions, Fig. 5a has been developed. Although the data were not obtained at constant subcooling, nor is one complete set of data by a single investigator available. Fig. 5a does suggest a trend of increasing degree of fragmentation with increasing drop radius for tin within the radius range of 0.22 to 0.50 cm.

2.5 Central Internal Voids. In the experiments of Flory et al [15] (and also in Bradley's experiments on thermal fragmentation of a hot molten jet [18]), hollow voids were observed in the interior of solidified, unfragmented, originally hot material. This, in conjunction with the observed outward burst of metals, indicates internal pressure generation in the hot molten material prior to fragmentation.

It must be noted that, in general, the spread in the fragmentation data for experiments conducted under nominally identical conditions is large. However, in the experiments of Cho [14,17] the trends have been obtained by averaging the results of at least five experiments performed under identical test conditions.

3. DISCUSSION OF PREVIOUSLY ADVANCED MECHANISMS

Numerous physical mechanisms have been suggested to explain the free-contact mode of fragmentation. Table 1 summarizes these mechanisms. Some of these mechanisms are discounted by experimental observations as pointed out in

the following.

3.1 Shell Solidification. Fragmentation may be postulated to result from pressurization of the molten core of the hot material due to shrinkage of the solidifying surface. This mechanism, however, is incapable of explaining the observed fragmentation of bismuth in water [13-14], since bismuth is a ductile material and would plastically deform and blunt each propagation. Furthermore, the fragmentation of hot mercury (melting point-38.8°C in water [13] is also inexplicable by this mechanism.

3.2 Coolant Encapsulation. Fragmentation has been suggested to result from the evaporation of an amount of coolant that penetrates the molten material [15,19,20]. There is difficulty, however, in defining the mechanism by which the coolant penetrates the molten material which, in many cases, is at a temperature higher than the critical temperature of the coolant (e.g., tin at 500°C fragments in 20°C water while the water critical temperature is 373°C). At such high temperatures, mere contact of the liquid coolant with the molten material induces spontaneous nucleation in the coolant.

Sallack [19] suggested coolant encapsulation takes place in cracks in the solidifed surface.

Flory et al [15] suggested encapsulation of coolant is due to the development of surface instabilities in the molten material. The ripples formed at the molten surface

by these instabilities, called Helmoltz instabilities, were of small size. Even when liquid coolant is assumed to be encapsulated within the ripples, the penetration of the coolant would be too small to explain the central cavities observed by Flroy et al [15].

Board et al [20] have recently suggested that penetration of a jet of coolant into the hot molten material may result when a vapor blanket collapses at molten surface. Depending on the conditions, the scale of the jets and the corresponding depth of penetration may be small. The time scale of mixing between the jet and the molten material is based on the model of Plesset and Chapman [21]. Based on their own experiments, Board et al. postulate that a small disturbance can escalate by successive vapor growth and collapse cycles to generate significant interaction leading to a large explosion. This proposed mechanism is under continued development but the authors have not yet presented the results of testing it against the range of existing data.

3.3 Acoustic Pulse in the Coolant. It has been suggested [22] that fragmentation may be associated with the pressure pulse that develops in the liquid coolant due to instantaneous heating of the coolant at the interface with the hot molten material. If a constrained volume of liquid suddenly undergoes a temperature change at ΔT, the pressure in the liquid volume is changed by an amount of ΔP given by

$$\Delta P = \left(\frac{\partial P}{\partial T}\right)_v \Delta T. \qquad (1)$$

If perfect contact is postulated between the hot material (initially at a temperature T_1) and the coolant (initially at a temperature T_2), the interface temperature, T_{in}, assumes an intermediate value that may be calculated considering each of the materials is semi-infinite. The interface temperature is found to be constant in time and given by

$$T_{in} = T_1 - \frac{\sqrt{(\rho kc)_2}}{\sqrt{(\rho kc)_1} + \sqrt{(\rho kc)_2}} (T_1 - T_2) \qquad (2)$$

Thus at the time of contact, the coolant at the interface develops a pressure increase given by

$$\Delta P = \left(\frac{\partial P}{\partial T}\right)_v (T_{in} - T_2) = \left(\frac{\Delta P}{\Delta T}\right)_v \left[\frac{\lambda}{1+\lambda}\right] (T_1 - T_2) \qquad (3)$$

where $\lambda = \sqrt{(\rho kc)_1 / (\rho kc)_2}$. (4)

This pressure pulse at the interface propagates into the coolant as a pressure wave, and the pressure at the interface is reduced very rapidly. (The acoustic velocity in water is 1500m/sec at 20° C and in sodium is 2500 m/sec at 550° C.) From Eq. (3) it is clear that the pressure pulse developed at the interface of a certain combination of hot and

cold materials would be larger the larger is the difference $(T_1 - T_2)$. It is then expected that the extent of fragmentation by this mechanism, for a certain material combination, would increase proportional to $(T_1 - T_2)$. This is contradictory to the observed decrease in the fragmentation of stainless steel (initially at 2200° C) in sodium as the sodium temperature increases above 200° C in the experiments of Swift and Pavlik [12] and as the sodium temperature increases between 400° C and 600° C in the experiments of Armstrong [3].

3.4 Spontaneous Nucleation of the Coolant. It has been suggested that if the interface temperature defined by Eq. (2) is higher than the spontaneous nucleation temperature of the coolant, the high localized pressures resulting from the nucleation in the coolant would also extensively fragment the hot material [24]. In Table 2 the spontaneous nucleation temperatures are compared to the interface temperatures for the conditions of some fragmentation experiments. It is evident that for molten uranium dioxide and stainless steel in sodium the interface temperatures are much below the spontaneous nucleation temperature, and hence the observed fragmentation cannot be explained by this mechanism.

3.5 Vapor Bubble Growth and Collapse. Vapor bubble growth and collapse at the surface of the molten materials have been suggested to induce free-contact fragmentation [25].

This mechanism is incompatible with the observed fragmentation of molten metals in water when the metal-water interface is at temperatures higher than the critical temperatures of water.

For sodium, Judd [16] has shown that the pressure pulse generated by the collapse of a vapor bubble is higher for lower temperatures of sodium. Thus an association of fragmentation with the pressure pulses of the collapsing bubbles predicts an increase in the extent of fragmentation of stainless steel at lower sodium temperatures, contrary to the observed trend of fragmentation at large subcoolings of sodium.

3.6 Summary - In view of the foregoing discussion of mechanisms for the free-contact mode of fragmentation, no mechanism has been presented to date in a sufficiently convincing manner to explain the bulk of existing free-contact fragmentation data. It may be possible to adopt the position that this mode of fragmentation is due to a combination of the postulated mechanisms, each responsible for a given set of the data. However, our analysis of the existing data and the fragmentation phenomenon has led us to postulate an additional mechanism which appears consistent with all the observed experimental trends. This mechanism extends our previous [23] view, which suggested a necessary but insufficient criterion for fragmentation.

4. A PROPOSED MECHANISM OF FRAGMENTATION

The free-contact mode of fragmentation is proposed here to be the result of growth of bubbles generated by internal

acoustic cavitation within the hot molten material. Acoustic cavitation is suggested to result from pressure waves induced within the hot drops due to the pressure pulsations at the surface of the hot molten drops due to the pressure pulsations at the surface of the hot molten drop resulting from its sudden immersion in a cool pool.

Experiments of rapid heating of metallic surfaces submerged in water have shown that transient vapor film formation is accompanied by high frequency pressure pulses [27,28]. Such pressure pulsations at the surface of a quenched molten drop will result in pressure waves inside the drop. Thus, the internal molten material will be subjected to an oscillating pressure field. The possibility of inducing cavitation in a liquid by an oscillatory pressure field has been well demonstrated in experiments involving the application of high intensity sound fields to several liquids [29-31].

The required negative pressure fields to achieve acoustic cavitation in practice seems definitely not the theoretical levels obtainable from the results of Bernath [32] which are derived from the work of Volmer [33]. For the hot drop materials at the temperatures of interest, these theoretical (negative) cavitation pressures which are directly proportional to surface tension are all tens of thousands of atmospheres [34]. Rather, experimental efforts [35] to achieve negative pressures in water and in mercury have shown that even under

scrupulously controlled laboratory conditions, negative pressures of only a 5th to a 50th of the theoretical pressures could be achieved before cavitation occurred. Additionally, cavitation in the experiments cited above [29-31] occurred at pressures far less than the theoretical negative levels. It is plausible to assume therefore that for the hot drop experiments we are analyzing in which experimenters have not reported any efforts to degas the hot drops prior to test, noncondensable gases which can serve as heterogeneous nucleation sites are present in the liquid drops.

The proposed mechanism is capable of explaining several of the previously unexplained trends of fragmentation summarized in Section 2, as will be discussed. It is necessary to examine analytically the effects of the experimental conditions on the potential for acoustic cavitation and subsequent bubble growth and then compare these trends with those observed for the fragmentation behavior. Thus we will examine first the pressure characteristics of the transient vapor film formation at the surface of the molten material (Section 5). Then, the development of interior pressure waves in the hot molten material resulting from the pressure pulsations at the molten material surface is examined (Section 6). Finally, the expected trends of both acoustic cavitation and bubble growth within the molten drops is compared to the experimental trends of fragmentation (Section 7).

5. CHARACTERISTICS OF THE PRESSURE PULSATIONS OF VAPOR FILM FORMATION

The authors [29] have developed a model to describe the dynamic formation of a vapor film at the surface of a hot sphere which has suddenly been immersed in a coolant. This model has been used to investigate the characteristics of the pressure pulses accompanying vapor film formation for conditions depicting some of the reported dropping experiments. The investigated cases of hot drops in water and hot drops in sodium are summarized in Tables 3 and 4, respectively.

The pertinent results of the study can be summarized as follows. In all cases the rapid vaporization initially results in a pressure rise in the film which accelerates the film/liquid interface. However, the outward motion of the interface continues beyond the equilibrium position (where the film pressure is equal to the ambient pressure). Thus the film pressure falls below ambient leading to deceleration of the interface. The film/liquid interface motion is then reversed, and the film starts to collapse. The continued evaporation in the film leads to a pressure rise in the collapsing film and the collapse is stopped before sphere/liquid contact is achieved. The cycle of growth followed by partial collapse is repated several times with decreasing amplitude of the pressure fluctuations. The amplitude and frequency of the film pressure oscillation depend on the conditions of interaction and are typically illustrated in

Figure 6 for the conditions of case 5. As Figure 6 illustrates the absolute magnitude of the pressure pulses is very dependent on the assumed initial film thickness. For the hot liquid metal drops under consideration it is reasonable to assume that initial gas films of the order 10^{-5} cm thick or smaller are experimentally present. If the layer of non-condensable gas swept in with the hot liquid metal drop as it enters the pool were a monomolecular layer, it could be as thin as 10^{-8} cm which forms a natural limit for this parameter. An initial film thickness of 10^{-5} cm was assumed for the cases calculated in [39] and summarized below:

5.1 Effect of Cool Pool Temperature - For the pressure histories of cases 1, 2 and 3 which have water pools, the first pulse (positive with respect to ambient) increases with the increase in the water temperature, although subsequent pressure pulses are damped quickly. Also the amplitude and frequency of the negative pressure pulses subsequent to the first positive pulse are greater the lower the water temperature. The amplitude behavior of the initial negative pulse illustrated on Fig. 2b exhibits a trend similar to the comparable experimental data of Fig. 2a.

For sodium pools, cases 14 through 17, the higher the sodium temperature, the higher is the first positive pressure pulse, similar to the water cases. However, the negative pressure pulses subsequent to the first pulse demonstrate maximum magnitude for an intermediate sodium subcooling.

The amplitude of the initial negative pulse, illustrated on Fig. 3b, also exhibits a trend similar to the comparable experimental data of Fig. 3a.

5.2 Effect of the Drop Temperature. In both water and sodium analysis of cases 1, 4 and 5 indicated that the increase in the initial temperature of the drop leads to higher pressure pulses in the film. The frequency of pulsation, however, is decreased by the increase in the initial drop temperature. The trend of the amplitude of the initial negative pressure pulse is illustrated on Fig. 4b and exhibits behavior similar to the comparable experimental data of Fig. 4a.

5.3 Effect of the Drop Radius. Under the same conditions of materials and temperatures of both the drop and the coolant, analysis of cases 8, 9 and 10 indicated that an increase in the drop radius leads to enhancement of the amplitude of the pressure pulses. However, the frequency of the pulses is decreased by the increase of the sphere radius. Again the amplitude behavior of the initial negative pulse is illustrated on Figure 5b and exhibits a trend similar to the comparable experimental data shown on Figure 5a.

6. INTERIOR PRESSURE WAVES

6.1 Analytic Solution Method in the Hot Drop. In this section we take up the calculation of the interior pressure wave under the influence of the pulsating film on the surface calculated in the previous section.

The interior pressure obeys the wave equation in the small velocity approximation with viscosity effects as given in Eq. (5):

$$\nabla^2 p = \frac{1}{c^2}\left(\frac{\partial^2}{\partial t^2} - \varepsilon c \frac{\partial}{\partial t}\nabla^2\right)p \tag{5}$$

$$\text{where } \varepsilon = \frac{(\eta + 4/3\mu)}{\rho c} . \tag{6}$$

Introducing the Fourier transforms of p and f (a volume source term) we obtain

$$\nabla^2 p_\omega + K^2 p_\omega = f_\omega \tag{7}$$

$$\text{where } K^2 = \frac{k^2(1-i\varepsilon k)}{(1+\varepsilon^2 k^2)} = \frac{k^2}{1 + i\varepsilon k} \quad \text{and } k = \frac{\omega}{c} . \tag{8}$$

The result then of the viscous terms is to make the wave number, k, complex indicating attenuation of the wave.

Equation (7) has two inherent approximations which should be recognized. First, it is a small velocity approximation whose application here can be justified by the small compressibility of the liquid droplet materials and the moderate resulting frequencies calculated. Second, it is for an adiabatic wave which may not be an especially good approximation when the thermal conductivity of the material (i.e., a liquid metal) is high. Nonetheless we will use these equations in the expectation that we can find essentially the right trends in the phenomena and later work can correct the

approximations as judged necessary.

Next we outline the methods used to find the pressure time histories. We begin with one of Green's theorems for the Fourier Transform of p :

$$P_\omega = \int_{V_o} f_\omega G_\omega \, dV_o + \int_{S_o} \left[G_\omega \frac{\partial}{\partial n_o} p_\omega - p_\omega \frac{\partial}{\partial n_o} G_\omega \right] ds_o \qquad (10)$$

where n_o is the outward pointing normal and G is the appropriate Green's function, i.e.,

$$G_\omega = g_\omega(\bar{r}, \bar{r}_o) + \chi \qquad (11)$$

$$\text{where } \nabla^2 \chi + K^2 \chi = 0 \qquad (12)$$

$$\text{and } \nabla^2 g_\omega(\bar{r}, \bar{r}_o) + K^2 g_\omega(\bar{r}, \bar{r}_o) = -\delta(\bar{r}, \bar{r}_o) \qquad (13)$$

where $\bar{r}$ is the field point and $\bar{r}_o$ is the source point.

The term χ is added in Eq. (11) so that G_ω satisfies the boundary conditions at the surface of the sphere.

In the particular case being considered, we believe that the dominant source of the acoustic wave is an applied pulsating pressure at the surface of the sphere. It should therefore be sufficient to consider only the surface terms and so we set $f_\omega = 0$). We can make the further simplifying assumption that the surface of the sphere is a rigid boundary. This requires that $G_\omega(a) = 0$. Using these two assumptions gives:

$$p_\omega(\bar{r}) = -\int p_\omega(a) \frac{\partial}{\partial n_o} G_\omega \, ds_o. \qquad (14)$$

Now the Green's function for an infinite medium is

$$g_\omega = \frac{iK}{4\pi} \; h_o(KR) \tag{15}$$

where h_o is a zero order spherical Hankel function and

$$R = \left|\bar{r} - \bar{r}_o\right| \; . \tag{16}$$

By expanding g_ω and X in spherical coordinates, applying the boundary conditions and performing the angular integration in Eq. (14) we get

$$p_\omega(r) = p_\omega(a) \; \frac{j_o(Kr)}{j_o(Ka)} \; . \tag{17}$$

To obtain the desired pressure time history it is only necessary to invert the transform to obtain

$$p\ (r,t) = \int_{-\infty}^{\infty} \frac{j_o(Kr)}{j_o(Ka)} \; p'_\omega(a) \; e^{-i\omega t} \; d\omega \; . \tag{18}$$

It is also useful to have an explicit expression for p(r,t) at r=0, which is

$$p(o,t) = \int_{-\infty}^{\infty} \frac{Ka}{\sin Ka} \; p_\omega(a) \; e^{-i\omega t} \; d\omega \; . \tag{19}$$

Calculation of the interior pressure wave can now be accomplished given the pressure at the surface. Numerically this has been accomplished by the use of the Fast Fourier Transform (FFT) method due to Cooley and Tukey [26], which is available as a FORTRAN subroutine called FOURT [37]. It has been used to calculate the forward transform as in Eq. (9) and the inverse transform as in Eqs. (18) and (19). The solution P expressed in Eq. (18) has some practical limitations in

addition to those imposed by the various assumptions which have been outlined. The most important limitation is that, as the wave lengths involved become much smaller than the radius of the sphere, the solution has many maxima and minima which require a large number of finely spaced time steps over which p(a,t) must be known. Further, more and more significant figures must be carried in order to get meaningful results. It is also necessary that checks are provided to ensure that the range of wavelengths for which this method is useful is being obtained in the numerical work. The maximum value of the real part of Ka in this work was approximately 40 and is near the upper limit for which this method is generally useful. Another check for the accuracy of the solutions can be applied to the imaginary part of p(r,t), which must be as small as possible. This is because both the real and imaginary parts of p satisfy the wave equation; and, since the value of the imaginary part is zero initially, it must also be zero at all subsequent times. In the results obtained to date, the imaginary part of p(r,t) has been a factor of 10^5 smaller than the real part in all cases.

6.2 Numerical Results. In this section the numerical results for various cases of Table 1 will be discussed. In all of the results to be discussed only the short time (5×10^{-5} sec or less) interior pressure history needed to be calculated, since it was only in this time domain that the

driving surface pressure curve was found to resonate within the sphere. The later time domains of 10^{-4} to 10^{-3} sec do not exhibit resonance behavior, since the driving surface pressure oscillations are of low frequency. Thus, in the later time domain, which for the sphere-pool systems investigated represents a low frequency, long wavelength limit, the pressure history of the interior wave is the same as the surface pressure history. This can be seen analytically by taking the limit as $k \to 0$ of Eq. (17) to obtain:

$$\lim_{k \to 0} p_\omega(r) = \lim_{k \to 0} p_\omega(a) \frac{a \sin(kr)}{r \sin(ka)} = p_\omega(a). \qquad (20)$$

The most significant parameter utilized in obtaining these results was ε, the sum of the two viscosity coefficients. Exact values of ε applicable to the hot liquid drop are not known. The following results for the center of the sphere were obtained utilizing a value of .02 cm, which should represent an overestimate thereby tending to underpredict the magnitude of the pressure pulses within the initial liquid drop.

6.2.1 Effect of Coolant Temperature. The effect of increasing the temperature of the water was investigated in cases 1, 2 and 3, which correspond to temperatures of 20, 50 and 80° C. The results of the center of the sphere, r = 0, are shown in Fig. 7. Here the amplitude of the interior drop pressure swings increases with increasing pool temperature.

This happens because of the increase in the peak pressure at the surface together with the constant rise times for the pool temperature cases investigated. However, this effect is in marked contrast to the experimental data in which fragmentation is decreased as the pool temperature is increased.

6.2.2 Effect of Hot Drop Temperature. The results of the pressure time history calculations within the hot sphere shown in Fig. 8 for $\delta = 0$ and $a = .3$ cm were carried out at hot sphere temperatures of 400, 500 and 700°C, corresponding to cases 4, 1 and 5. It was found that, as the temperature increases, the amplitude of the interior pressure waves (both positive and negative swings) gets larger. In all cases the pressure becomes negative but only for short periods (on the order of 1 microsecond). For this variable of hot sphere temperature, the trends of the calculations are consistent with the associated fragmentation data.

6.2.3 Effect of Hot Drop Radius. In Fig. 9, the pressure time history within the hot sphere at $r = 0$ for cases 9, 5 and 10, corresponding to $a = .1$, .3 and 1.0 cm is shown. The trend here is for the absolute value of the pressure to increase quite dramatically with increasing drop radius. This is not only because the initial pressure pulse at the surface is increasing, but also because the resonant resonse of the sphere is increasing. Since the likelihood of cavitation increases with more negative pressure, the trend of these

calculations is consistent with the fragmentation data reviewed earlier, i.e., the extent of fragmentation increases with hot sphere radius.

6.2.4 Uncertainties in Prediction of Negative Interior Pressures. The absolute magnitude of the calculated negative interior pressure pulses are subject to the following key uncertainties. The driving condition, the surface pressure, is very sensitive to the assumed thickness, , of non-condensable gas on the hot drop surface. Additionally, the interior pressure analysis is based on the approximations previously discussed plus the assumption of the spherically shaped drop. While the net effect of all these assumptions is not yet established, these effects are thought to be secondary to the effect of viscosity. The value of viscosity utilized, .02 cm, was selected to yield a conservative lower bound for the magnitudes of the pressure pulses in the initially all-liquid drop.

7. THE PROPOSED ACOUSTIC CAVITATION-BUBBLE GROWTH MECHANISM FOR FREE-CONTACT FRAGMENTATION

The results of the previous section demonstrate that negative interior pressures can be generated with magnitude sufficient to generate bubbles by acoustic cavitation. It would be tempting to postulate that droplet fragmentation is caused directly by the onset of acoustic cavitation. If this were so, the extent of fragmentation would seem to be

directly proportional to the negative droplet pressure achieved. However, such a consistency in trend between experimentally observed fragmentation and negative droplet pressure was not obtained with pool temperature as a test variable as illustrated on Fig. 7. On the other hand, as Figs. 2 through 5 illustrate, consistency between fragmentation data trends and the minimum vapor film pressure were obtained for all the test variables investigated. Thus we are lead to postulate that the mechanism of fragmentation is dependent upon the aspect of bubble behavior initially most dependent on vapor film pressure is the extent of bubble growth.

Subsequent to cavitation it appears that the bubble will first grow and then start to collapse. The generation of the cavitation bubble will significantly affect the viscosity of the liquid drop and severely damp the subsequent interior pressure waves. Thus the solutions of Figs. 7-9 would be valid only until cavitation occurred, and the subsequent interior pressure history would follow the surface pressure history. A typical resultant interior pressure history is shown on Fig. 10 using case 5 as the example. Note that in Fig. 10 the time scale is linear, which depicts the surface pressure history of case 5 as a sharp positive pulse followed by a prolonged negative pressure over the short time domain shown.

For these conditions bubble growth will be initiated after

cavitation with liquid vaporization occurring at the bubble-liquid interface. However, since the liquid metal droplet vapor pressures at the applicable liquid temperatures are so low (10^{-6} mm mercury at 700° C for tin), it appears probably that even for low initial film thicknesses, , the resultant surface pressures will exceed the equilibrium bubble pressures. Therefore bubble collapse will follow bubble growth. It is possible that the actual mechanism for droplet fragmentation may be some combination of the oscillatory growth-collapse behavior. However, the extent of growth is affected by the difference of $P_\infty - P_{f,min}$, the ordinate of Figs. 2b-5b, in that manner directly consistent with the fragmentation data of Figs. 2a-5a; i.e., the larger the parameter $P_\infty - P_{f,min}$, the more growth, the more observed extent of fragmentation. Thus, pending calculation of detailed behavior of the growth-collapse behavior of the bubble subsequent to cavitation, we hypothesize that fragmentation is induced by bubble growth subsequent to cavitation.

The proposed hypothesis for fragmentation is consistent with the experimental observation of hollow voids by Flory et al [15] mentioned earlier which indicated the occurrence of internal pressure generation in the hot droplets prior to fragmentation. Also comparison of the results of ANL experiments [14] on aluminum, zinc, lead and bismuth dropped into 20°C water are of interest with respect to his hypothesis. In these experiments, aluminum (σ = 900 dynes/cm) and zinc

(70 dynes/cm) did not fragment, whereas lead (400 dynes/cm) and bismuth (350 dynes/cm) did fragment with the bismuth fragmentation being more extensive than that of lead. These results demonstrate the expected decrease in fragmentation with increased surface tension, which would be observed if the tendency for fragmentation due to bubble generation and growth from a phenomena like acoustic cavitation was resisted by increased hot drop surface tension.

8. SUMMARY AND CONCLUSIONS

A mechanism that explains several of the observations of fragmentation of hot molten drops in coolants has been investigated. The mechanism relates the fragmentation to the development of acoustic cavitation and subsequent bubble growth due to severe pressure excursions within the hot material resulting from the pressure pulses accompanying coolant vaporization at the sphere surface.

The characteristics of the pressure pulses accompanying vapor film growth at the surface of a hot molten drop suddenly immersed in a coolant pool have been determined for conditions depicting reported dropping experiments. A key uncertainty relative to the calculated surface pressure history is the initial thickness of noncondensable gas at the hot drop surface. Next, a model describing the pressure field inside a molten drop as a result of the pressure pulses at the drop surface was developed. This model predicts that strong

pressure oscillations will be induced inside the molten drop due to the initial surface pressure pulse of short duration (2×10^{-6} sec). However, the longer duration surface pressure pulses seem not to induce large oscillations of pressure inside the hot drop. It could therefore be concluded that cavitation will be initiated by the high frequency pulsating internal pressure induced by the first surface pulse. The growth of the vapor nuclei inside the hot drop would be influenced by the subsequent long duration surface pressure pulses, since the subsequent interior pressure history of the hot drop directly follows the surface pressure history after cavitation occurs. Composite interior pressure histories of the type shown in Fig. 10 lead to postulated bubble generation (at about 8×10^{-6} sec) and growth trends (after 8×10^{-6} sec) which are consistent with observed trends in extent of fragmentation.

The hypothesis presented has been developed in terms of a two-parameter model of the pressure history of a hot sphere immersed in a coolant. The two parameters are δ, the initial film thickness, and ϵ, a sum of two viscosity components. The parameter, δ, essentially controls the amplitude of the surface pressure oscillations which is the driving function producing the interior oscillations, and ϵ determines the amplitude of the interior oscillations for the first pulses sufficient to cause cavitation.

The agreement of the predicted trends with the available

experimental results indicates that the proposed mechanism merits further consideration. The present work shows the importance of the initial film thickness as a parameter which has not been measured in past experiments. Even though it may be difficult to measure, it is still a convenient way to characterize the strength of the vapor film oscillations. Present work is being directed at measurements to confirm the calculated surface pressure histories. Analyses are planned to relax assumptions in the interior pressure walve solution method and to further investigate the dynamic bubble formation and growth processes to relate them directly to the fragmentation event.

SUPPLEMENT

The two general topics considered here are a review of the underlying assumptions of the acoustic cavitation model and an analysis of the available energy for fragmentation due to the proposed mechanism. Each subject is reviewed in light of subsequent analysis and comments by the authors and other interested persons.

REVIEW OF BASIC ASSUMPTIONS

Four assumptions are made in the development of the acoustic model. First the model considers a spherical molten drop becoming instantaneously immersed in a coolant pool and film boiling occurring. Reid [40] and others have suggested that these conditions are somewhat unrealistic, and could affect the results of the analysis. Suggestions have been made to relax these assumptions and account for irregular drop shape due to flow forces, and a finite immersion rate with an initially thick vapor blanket around the droplet. The second assumption is that the film pressure is assumed to be spatially uniform. Third the thickness of the film layer is parametrically varied between 10^{-4} cm and 10^{-6} cm. The pressure pulses generated within the film layer are largely dependent upon the thickness. Watson [41] suggests that smaller vapor thicknesses down to 10^{-8} be considered as feasible. Also during the initial stages of immersion the vapor layer could possibly be thicker than assumed in the past

analysis (10^{-3} cm). Finally during the short time of this interaction the convective heat transfer within the film and coolant are neglected. To avoid mathematical complexities the coolant pool is modeled under the two bounding cases: an incompressible liquid or a compressible acoustically infinite liquid. Watson [41] suggests that the limiting case of a compressible liquid of acoustically infinite extent ignores a substantial portion of the mechanical energy. It is lost from the vapor film by neglecting the fact that [realistically] it is transformed into gravitational potential energy (by the rising of the coolant level and its subsequent falling) which is transferred back to the vapor film over the cycle. Viscous losses in the tank could be ignored due to the small velocities.

AVAILABLE ENERGY FOR FRAGMENTATION

Under the conditions of the acoustic cavitation theory, energy is transmitted into the molten drop by pressure variations in a vapor film which surrounds the drop. The work done by this vapor film on its surroundings is the upper bound of the amount of energy that could possibly be transferred into the drop.

Using results obtained by Kazimi [34], the amount of work done by the film was calculated in a graphical-numerical manner. The calculation was done for case 14 (i.e., stainless steel drop temperature = 2200°C, sodium pool temperature = 850° C,

stainless steel drop radius = .035 cm) and is presented in Appendix I. During the first expansion the film does 3050 ergs of work.

However, it cannot be expected that all the work done by the film will be done on the molten drop; a certain fraction of the work will be done on the sodium pool as well. An estimate of the amount of energy transmitted into the drop was made based upon a formula developed by Caldarola and Kastenberg [42]. This formula is for the energy transmitted through a semi-infinite body by a pressure impulse from a small source on the edge of the body. The justification for applying this equation to the situation of a film around a molten drop is that the film can be considered to be a large number of small sources which transmit energy into both the molten drop and the sodium pool. This derivation is in Appendix II and shows that the partition of energy between the molten drop and the pool can be approximated in terms of the densities of the materials.

An expression for the radius of the drop material after fragmentation is derived in Appendix III. In Figure 11, a line of final radius versus energy transmitted into the molten drop is drawn for the conditions of case 14. Indicated on the line are points which correspond, according to the acoustic cavitation hypothesis, to the maximum possible amount of energy transmitted into the drop and the best estimate of the

amount of energy transmitted.

Experimental data on the fragmentation of stainless steel in sodium is presented in Appendix IV and also plotted in Fig. 11. Unfortunately the initial drop radius is smaller and the pool temperature is hotter for case 14 than for the conditions of the experimental data and direct comparison cannot be made. According to the acoustic cavitation hypothesis, the work done by the vapor film will increase with increasing drop radius and decrease with decreasing pool temperature. Therefore, the conditions of case 14 and the conditions of the experimental data may yield roughly the same work done by the film.

The calculation of the energy available for fragmentation shows that, if the acoustic cavitation theory is to account for the observed residual particle size, fragmentation cannot occur in one step. Even if all the work done by the film were done on the drop, the residual particle size after one fragmentation step is three to four times larger than the experimentally determined residual particle size. The best estimate of the work done on the molten drop indicates that many fragmentation steps would have to be made before the experimentally determined residual particle size is reached.

Another method of calculating the work done upon the molten drop is to establish an expression for the displacement of the drop surface due to the vapor film pressure. Watson [41] developed such an expression for energy as shown in

Appendix V. The Fourier transform of the velocity (4)(a)) of the interface is determined knowing the pressure. Then the velocity is found by the inverse transform Eq. (16). Using then the velocity and pressure (p(a) from Kazimi [34]), the work done on the molten drop is found over some time span (o to t) by integration and numerical evaluation. No numerical results have been obtained by this method.

In considering the possibility of numerous pressure pulse cycles to account for the final fragmentation size, Watson [14] suggested that the pressure pulse over each cycle is increased by the reflection of the pressure waves into the hot molten drop (see Appendix VI). At the gas-cold liquid interface there is a large impedance mismatch $P_g C_g \ll P_p C_p$ which causes very little of the pressure pulse to be transmitted to the cold liquid (and thus a small amount would be transmitted to the liquid). Likewise at the hot liquid-gas interface there is this same impedance mismatch allowing pressure pulses to be transmitted into the drop but not to be transmitted out. Subsequently over a few cycles the pressure becomes bigger and bigger within the film and hot drop. Finally this set of conditions in the hot drop could allow absorption of enough energy to overcome the surface energy to form by fragmentation, particle sizes comparable to experimental observation.

FUTURE WORK

Any additional work upon this proposed mechanism of acoustic cavitation should proceed along two major fronts. An overall view of the energy available for fragmentation due to the mechanism over many pressure cycles should be evaluated to determine if the mechanism can account for observed fragmentation sizes. If this overall energy view of the mechanism appears to be promising, then a relaxation of the underlying assumptions should be attempted.

ACKNOWLEDGEMENTS

This work in large part was supported by the Argonne National Laboratory and the U.S. Atomic Energy Commission.

NOMENCLATURE

c	speed of sound in the medium of specific heat
f	volume source term
k	wave number, ω/c, or thermal conductivity
K	defined by Eq. (8)
p	pressure fluctuation around some equilibrium pressure, P
r	bubble radius
s	surface
t	time
T	temperature
T^*	temperature for inception of film boiling by Henry's [28] correlation
v	volume
σ	surface tension
ϵ	effective viscosity (defined by Eq. 7)
δ	initial noncondensable vapor film thickness
η	coefficient of bulk viscosity representing a stress opposing the rate of change of compression
ρ	density
ω	frequency
μ	usual coefficient of viscosity

REFERENCES

1. Barghusen, J. J. et al, "LMFBR Nuclear Safety Program Annual Report," ANL-7800, July 1971, p. 321.

2. Amblard, M., et al, "Contact Effects Between Molten UO_2 and Sodium and Molten UO_2 and Water," EUFNR-811, March 1970.

3. Armstrong, D. R., Testa, F. J., and Raridon, D., Jr., "Interaction of Sodium with Molten UO_2 and Stainless Steel Using a Dropping Mode of Contact," ANL-7890, Argonne National Laboratory, December 1971.

4. Cho, D. H., et al, "Pressure Generation by Molten Fuel-Coolant Interactions Under LMFBR Accident Conditions," Proc. Conf. New Developments in Reactor Mathematics and Applications, CONF-710302, Idaho Falls, Idaho, March 1971.

5. Caldarola, L., "A Theoretical Model for the Molten Fuel-Sodium Interaction in a Nuclear Fast Reactor," Nucl. Eng. Design, Vol. 22, No. 2, October 1972, pp. 175-211.

6. Long, G., "Explosions of Molten Aluminum in Water - Cause and Prevention," Metal Progress, Vol. 71, May 1957, pp. 107-112.

7. Wright, R. W., "Kinetic Studies of Heterogeneous Water Reactors," TRW Space Technology Laboratories Report, STL-372-30, December 1965, pp. 62-74.

8. Darby, K., et al, "The Thermal Interaction Between Water and Molten Aluminum Under Impact Conditions In a Strong Tube," Proc. Conf. Eng. of Fast Reactors for Safe and Reliable Operation, Karlsruhe, October 1972.

9. Ivins, R. O., and Baker, L., "Chemical Engineering Division Semiannual Report, January-June 1964," ANL-6900, August 1974, pp. 270-280.

10. Teage, H. J., "Summary of the Papers Presented at the CREST Meeting on Fuel-Sodium Interaction at Grenoble in January and Report of Conference Papers 38 A-K on Fuel-Sodium Interaction," Proc. Conf. Eng. of Fast Reactors for Safe and Reliable Operation, Karlsruhe, October 1972.

11. Hinze, J. O., "Fundamentals of the Hydrodynamic Mechanism

of Splitting in Dispersion Processes," A. I. Ch. E. Journal, Vol. 1, No. 3, September 1955, pp. 289-295.

12. Swift, D., and Pavlik, J., "Chemical Engineering Division Semiannual Report, July-December 1965," ANL-7125, May 1966, pp. 187-193.

13. Witte, L. C., et al, "Rapid Quenching of Molten Metals," ORO-3936-6, August 1971.

14. Cho, D., and Fauske, H., Private Communication, Fall 1973.

15. Flory, K., et al, "Molten Metal-Water Explosions," Chem. Eng. Progress, Vol. 65, December 1969, pp. 50-54.

16. McCracken, G. M., "Investigation of Explosions Produced by Dropping Liquid Metals into Aqueous Solutions," UKAE Safety Research Bulletin 11, Spring 1973.

17. Cho, D., "LMFBR Nuclear Safety Program Annual Report: July 1969 to June 1970," ANL-7800, July 1971, p. 346.

18. Bradley, R. H., et al, "Investigation of the Vapor Explosion Phenomena Using a Molten-Metal Jet Injection into Distilled Water," ORO-3936-7, October 1971.

19. Sallack, J. A., "On Investigation of Explosions in the Soda Smelt Dissolving Operation," Canadian Pulp and Paper Association Meeting, Quebec, Canada, June 1955.

20. Board, S. J., et al, "Fragmentation in Thermal Explosion," Int. J. Heat and Mass Transfer, Vol. 17, No. 2, February 1974, pp. 331-339.

21. Plesset, M. S., and Chapman, R. B., "Collapse of an Initially Spherical Vapor Cavity in the Neighborhood of a Solid Boundary," J. Fluid Mechanics, Vol. 47, No. 2, 1971, pp. 283-290.

22. Cronenberg, A. W., "A Thermodynamic Model for Molten UO_2-Na Interaction Pertaining to Fast Reactor Fuel Failure Accidents," Ph.D. thesis, Nucl. Eng. Dept., Northwestern University, June 1971.

23. Kazimi, M., et al, "A Criterion for Free-Contact Fragmentation of Hot Molten Materials in Coolants," Trans. Am. Nucl. Soc., Vol. 15, No. 2, November 1972, p. 835.

24. Henry, R. E., and Cho, D. H., "Reactor Development Program Progress Report, December 1972," ANL-RDP-12, February 1973, p. 9.34.

25. "Reactor Development Program Progress Report, January 1966," ANL-7152, February 1966, pp. 90-96.

26. Judd, A. M., "The Condensation of Sodium Vapor Bubbles," AEEW-M813, UKAE-Reactor Group, Winfrith, 1968.

27. Wright, R. W., "Pressure Pulses in Rapid Transient Boiling," Trans. Am. Nucl. Soc., Vol. 6, No. 2, 1963, p. 338.

28. Board, S. J., et al, "An Experimental Study of Energy Transfer Processes Relevant to Thermal Explosions," Int. J. Heat & Mass Transfer, Vol. 14, October 1971, pp. 1631-1641.

29. Flynn, H. G., "Physics of Acoustic Cavitation in Liquids," in Physical Acoustics, Vol. 1, Part B, W. P. Mason, Ed., Academic Press, New York, 1964.

30. Sirotyuk, M. G., "Experimental Investigations of Ultrasonic Cavitation," in High Intensity Ultrasonic Fields, L. D. Rozenberg, Ed., Plenum Press, New York, 1971.

31. Knapp, R., Daily, J., and Hammit, F., Cavitation, McGraw Hill, New York, 1970, p. 293.

32. Bernath, L., "Theory of Bubble Formation in Liquids," Ind. Eng. Chem., Vol. 44, 1952, pp. 1310-1313.

33. Volmer, M., Kinetik der Phasenbildung, Theodore Steinkapft, Dresden and Leipsig, 1939.

34. Kazimi, M. S., "Theoretical Studies on Some Aspects of Molten Fuel-Coolant Thermal Interaction," Sc. D. thesis, Nucl. Eng. Dept., M.I.T., Cambridge, Mass., May 1973.

35. Hayward, A. T. J., "Negative Pressure in Liquids: Can it be Harnessed to Serve Man?", American Scientist, Vol. 59, No. 4, July-August 1971, pp. 434-443.

36. Cooley, J. W., and Tukey, J. W., "An Algorithm for the Machine Calculation of Complex Fourier Series," Mathematics of Computation, Vol. 19, April 1965, pp. 297-301.

37. Brenner, N., "FOURT," M.I.T. Information Processing Center Applications Program Series Report, Ap-7, revision 4.

38. Henry, R. E., "A Correlation for the Minimum Wall Superheat in Film Boiling," Trans. Am. Nucl. Soc., Vol. 15, 1972, p. 420.

39. Kazimi, M. S., Todreas, N. E., Lanning, D. D., and Rohsenow, W. M., "A Theoretical Study of the Dynamic Growth of a Vapor Film Around a Hot Sphere in a Coolant," Fifth International Heat Transfer Conference, Tokyo, 1974.

40. Reid, R. C., M.I.T., private communication, August 1974.

41. Watson, C. E., B&W, private communication, August 1974.

42. Caldarola, L. and Kastenberg, from the Appendix of "On the Mechanism of Fragmentation During Molten Fuel/ Coolant Thermal Interactions."

43. Armstrong, D. R., Tests, F. J., and Raridon, D., Jr., "Interaction of Sodium with Molten UO_2 and Stainless Steel Using a Dropping Mode of Contact," ANL/RAS 71-15.

44. Morse, P., Ingard, G., Theoretical Acoustics, M.I.T. Press

45. Watson, C. E., "Transient Heat Transfer Induced Pressure Fluctuations in the Fuel Coolant Interaction," M.I.T., Master's Thesis, 1974.

Table 1
Suggested Mechanisms of Free-Contact Fragmentation

1. Shell Solidification
2. Coolant Encapsulation:
   a. by cracks in a solidifying shell
   b. by Helmholtz instabilities
   c. by penetration of a coolant jet
3. Acoustic Pulse in the Coolant
4. Spontaneous Nucleation of the Coolant
5. Vapor Bubble Growth and Collapse
6. Cavitation within the Molten Material (Proposed in the present study)

Table 2

Comparison of Spontaneous Nucleation Temperatures of Sodium and Water with Temperatures at the Interface of Some Molten Materials* [3, 14]

Coolant (Temp., °C)	Molten Material (Temp., °C)	T_{in}, °C (Eq. 2)	$T_{s.n.}$, °C
Sodium (600)	UO_2 (2900)	1130	1850
	Stainless Steel (2200)	1346	1850
Water (20)	Pb (700)	543	314
	Bi (700)	543	314

*All the molten materials are reported to fragment under the experimental conditions.

Table 3

Values of the Parameters Varied for the Cases of Hot Spheres in Water[†]

Variables \ Case Number	1	2	3	4	5	6	7	8	9	10	11	12	13
Sphere Material	Sn	Sn	Sn	Sn	Sn	Sn	Sn	AgCl	Sn	Sn	Sn	Sn	Sn
Initial Sphere Temperature, °C	500	500	500	400	700	700	700	700	700	700	700	500	500
Water Pool Temperature, °C	20	50	80	20	20	20	20	20	20	20	20	20	20
Sphere Radius, cm	0.3	0.3	0.3	0.3	0.3	0.3	0.3	0.3	0.1	1.0	0.3	0.3	0.3
Initial Film Thickness, cm	10^{-5}	10^{-5}	10^{-5}	10^{-5}	10^{-5}	10^{-4}	10^{-6}	10^{-5}	10^{-5}	10^{-5}	10^{-5}	10^{-5}	10^{-5}
Coolant Compressibility I = incompressible C = compressible	I	I	I	I	I	I	I	I	I	I	C	C	C

[†]For all cases the initial film pressure and the ambient pressure are taken to be 1 atm.

Table 4

Values of Parameters Varied for the Cases of Hot Spheres in Sodium[†]

Variable \ Case Number	14	15	16	17	18	19	20	21
Sphere Material	SS	SS	SS	SS	UO_2	UO_2	UO_2	UO_2
Initial Sphere Temperature, °C	2200	2200	2200	2200	3200	3200	3200	3200
Sodium Pool Temperature, °C	850	800	600	250	850	800	600	800

[†]For all cases the sphere radius is 0.35 cm, the initial gas film thickness is 5×10^{-6} cm; the initial film pressure and ambient pressure are at 1 atm, and the liquid sodium is considered incompressible.

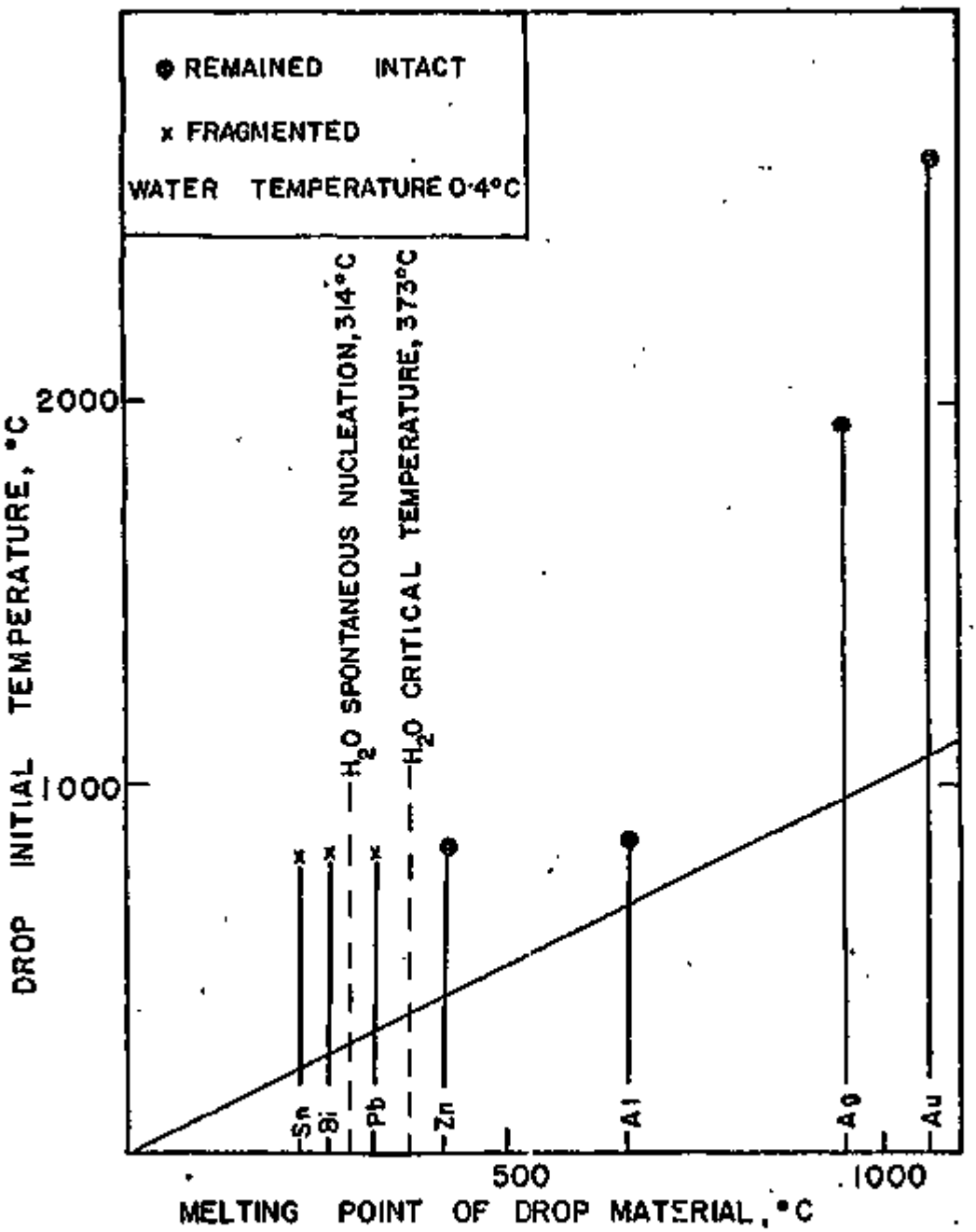

Figure 1. Results of Dropping Various Materials in Water (For Al, Ag, Au see Swift and Pavlik Ref. 12, for Sn, Bi, Pb and Zn see Cho Ref. 14).

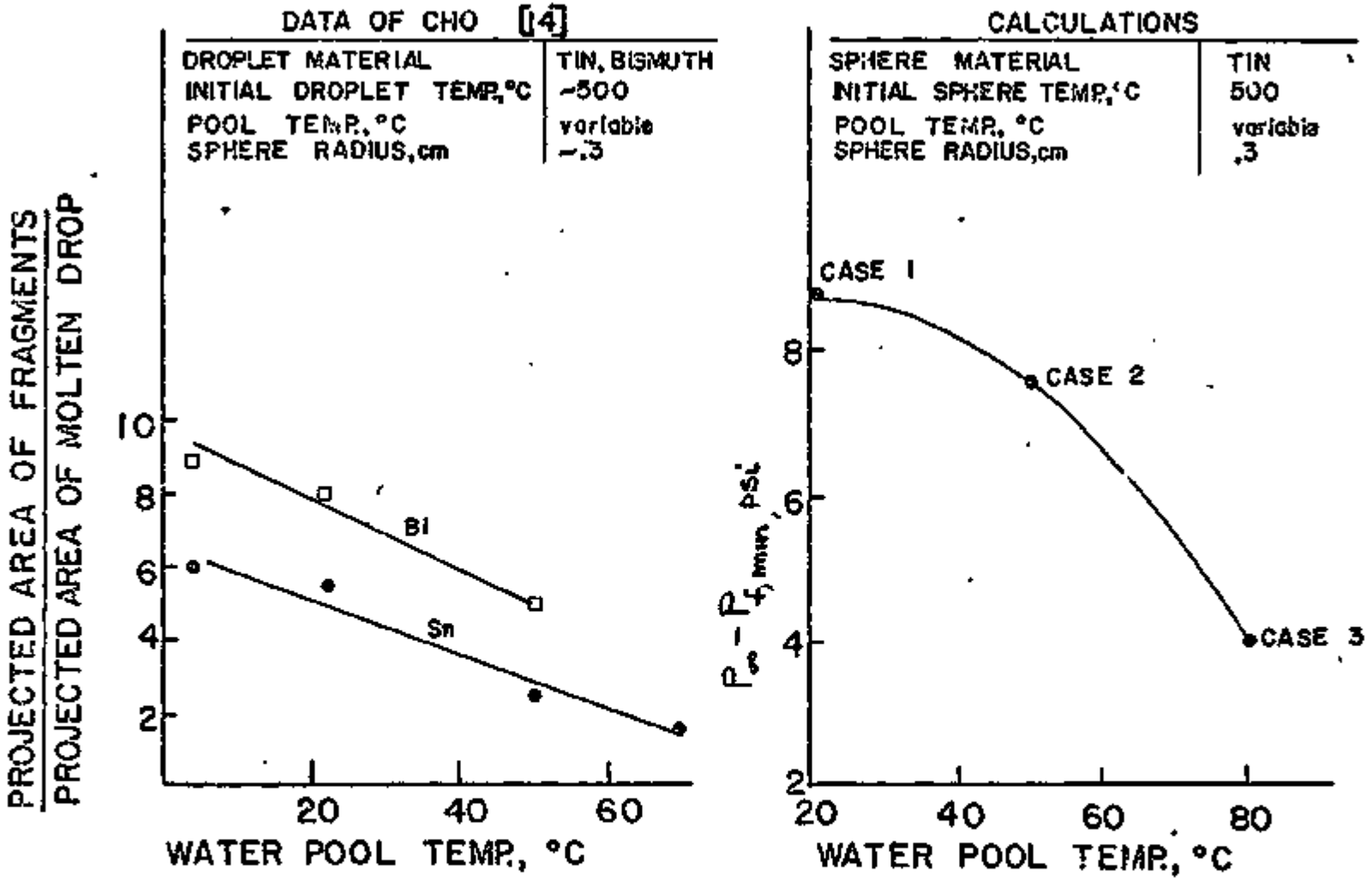

Figure 2. Comparison of the Effect of Water Pool Temperature on the Fragmentation of Molten Droplets in Water and on the Maximum Subatmospheric Pressure Reduction in a Vapor Film Growing Around a Hot Sphere in a Water Pool.

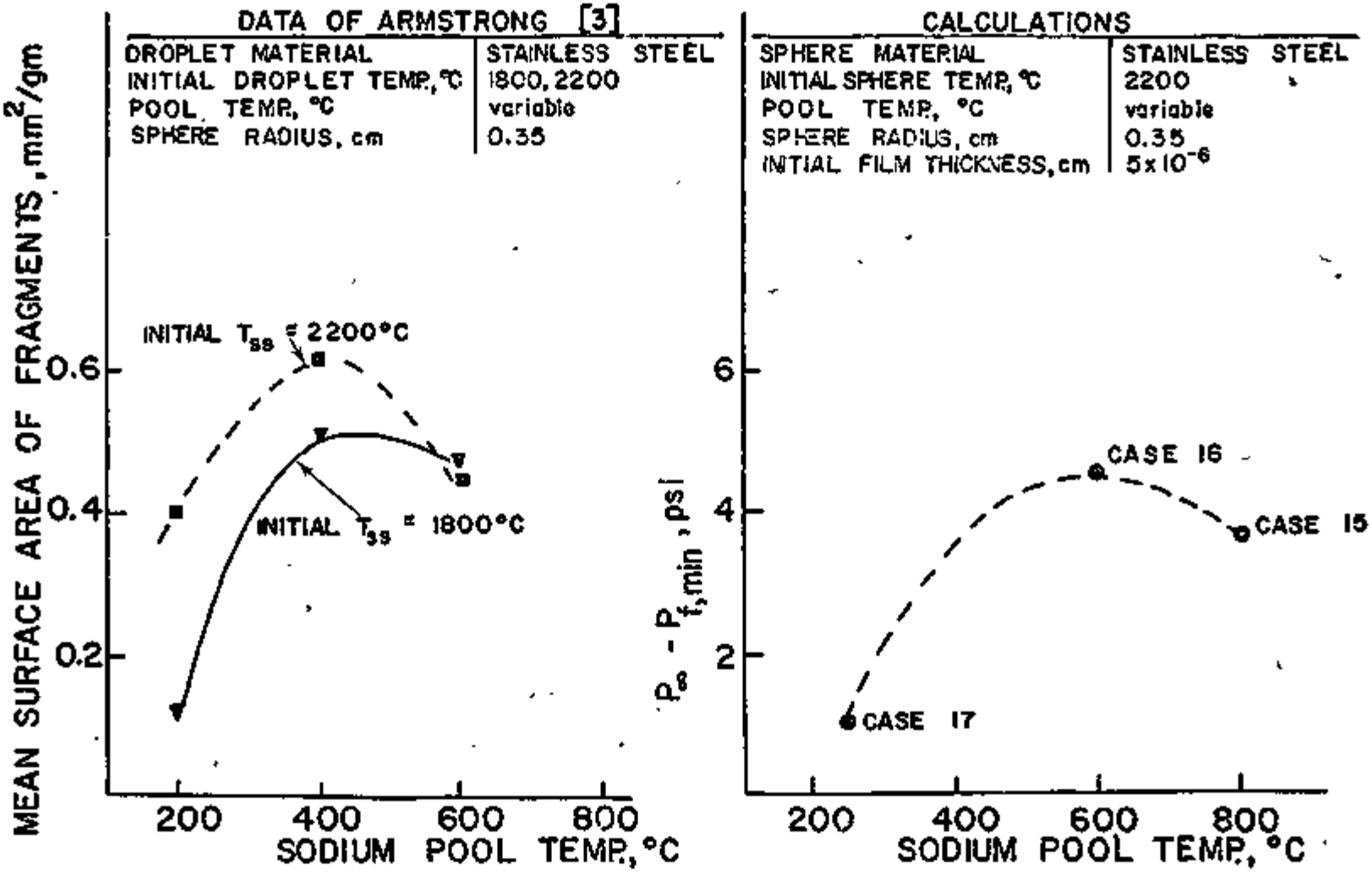

Figure 3. Comparison of the Effect of Sodium Pool Temperature on the Fragmentation of Stainless Steel in Sodium and the Maximum Subatmospheric Pressure Reduction in a Vapor Film Growing Around a Stainless Steel Sphere in a Sodium Pool.

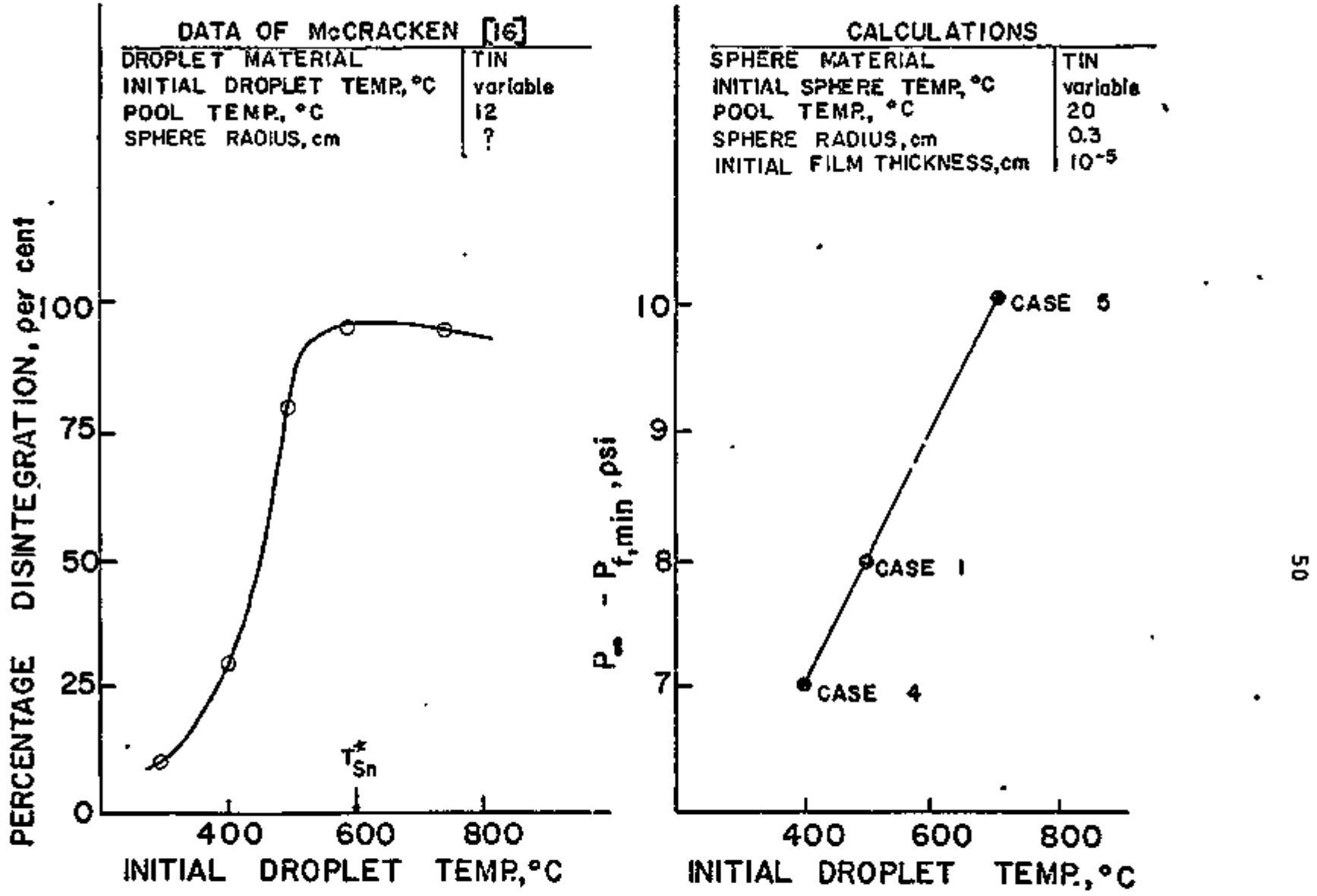

Figure 4. Comparison of the Effect of the Initial Temperature of the Hot Droplet on the Fragmentation in Water and the Maximum Subatmospheric Pressure Reduction in a Vapor Film Growing Around a Hot Sphere in a Water Pool.

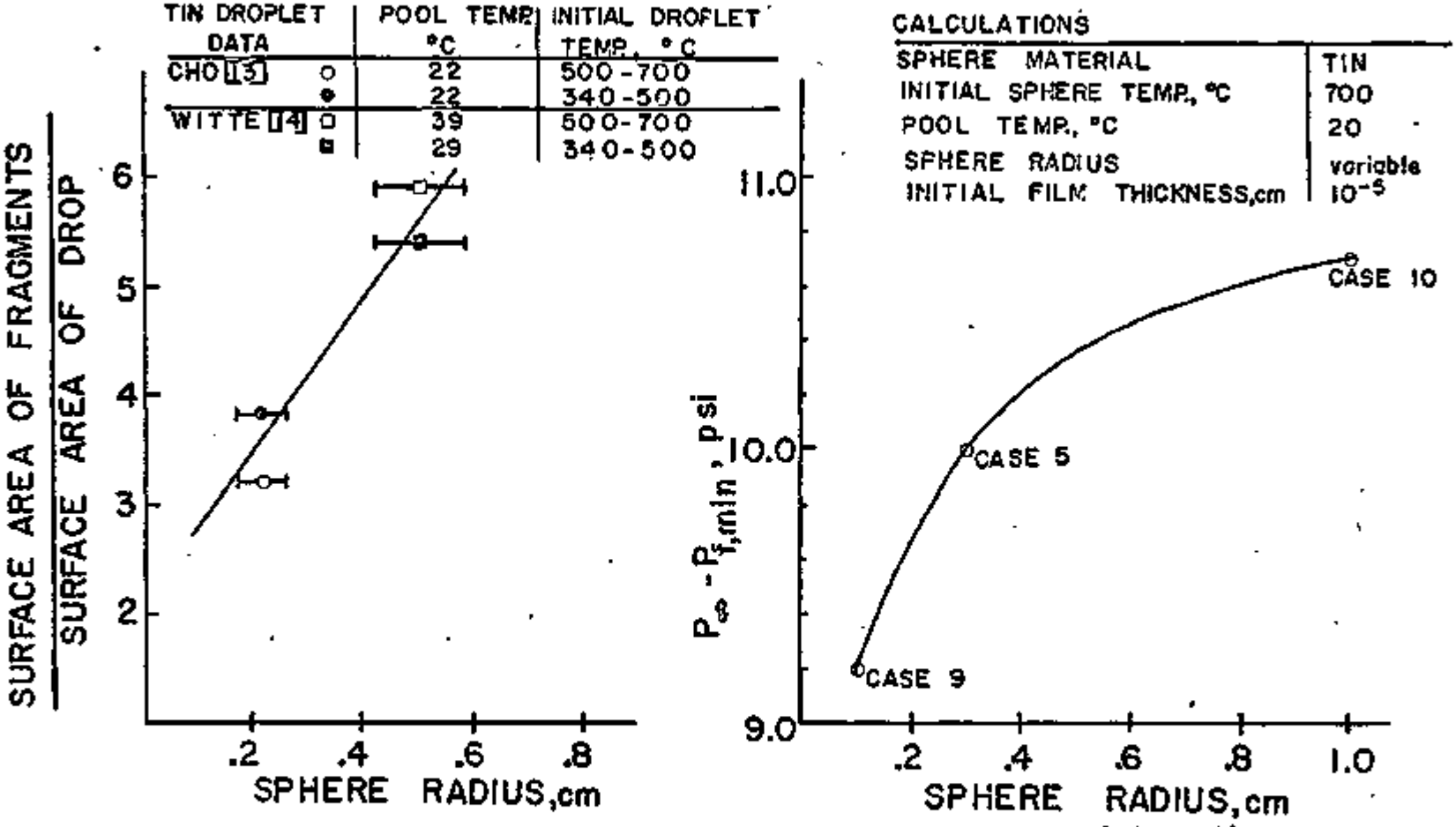

Figure 5. Comparison of the Effect of the Radius of the Hot Droplet on the Fragmentation in Water and the Maximum Subatmospheric Pressure Reduction in a Vapor Film Growing Around a Hot Sphere in a Water Pool.

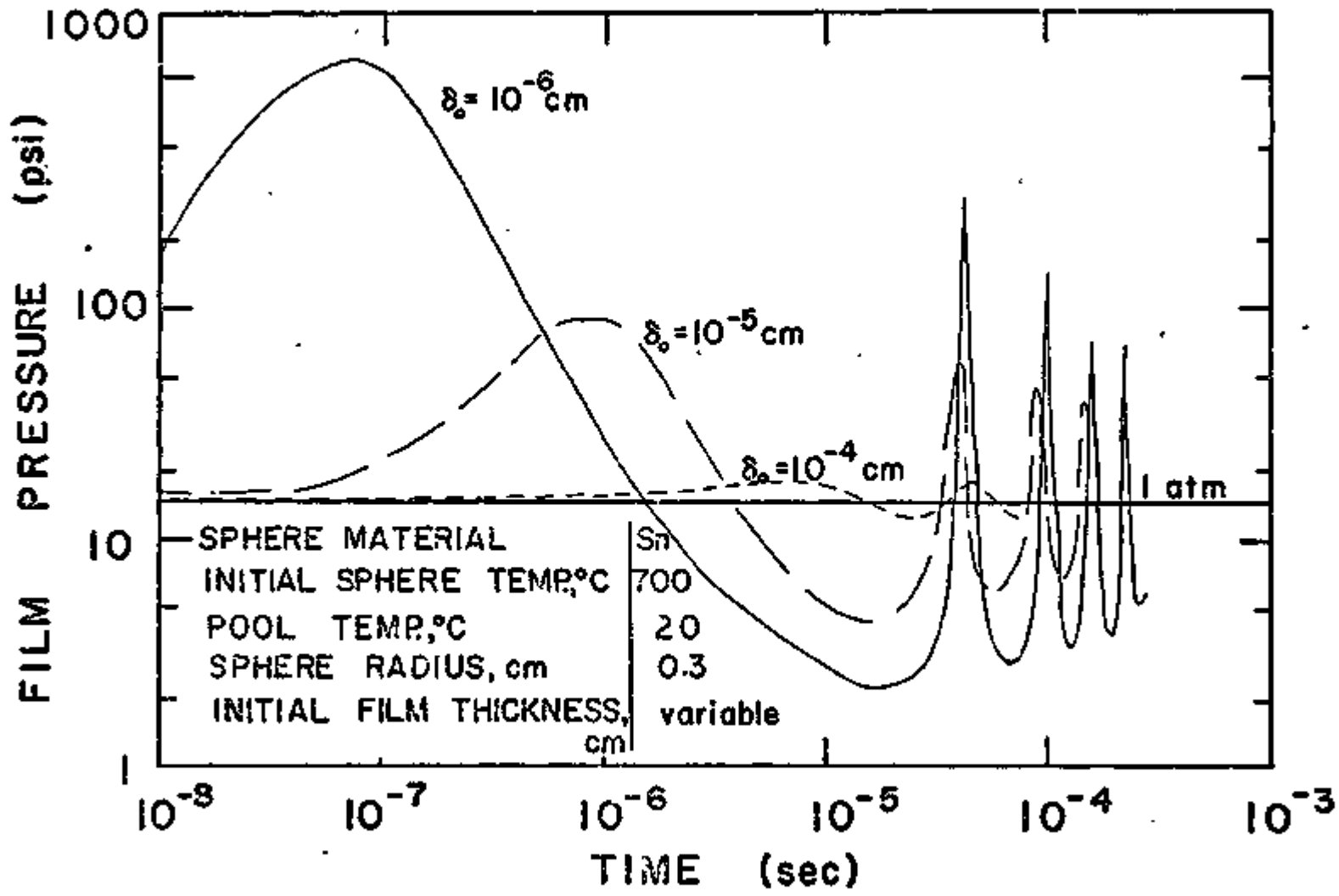

Figure 6. Effect of Initial Gas Film Thickness, δ_0 on Pressure-Time History of the Oscillating-Film.

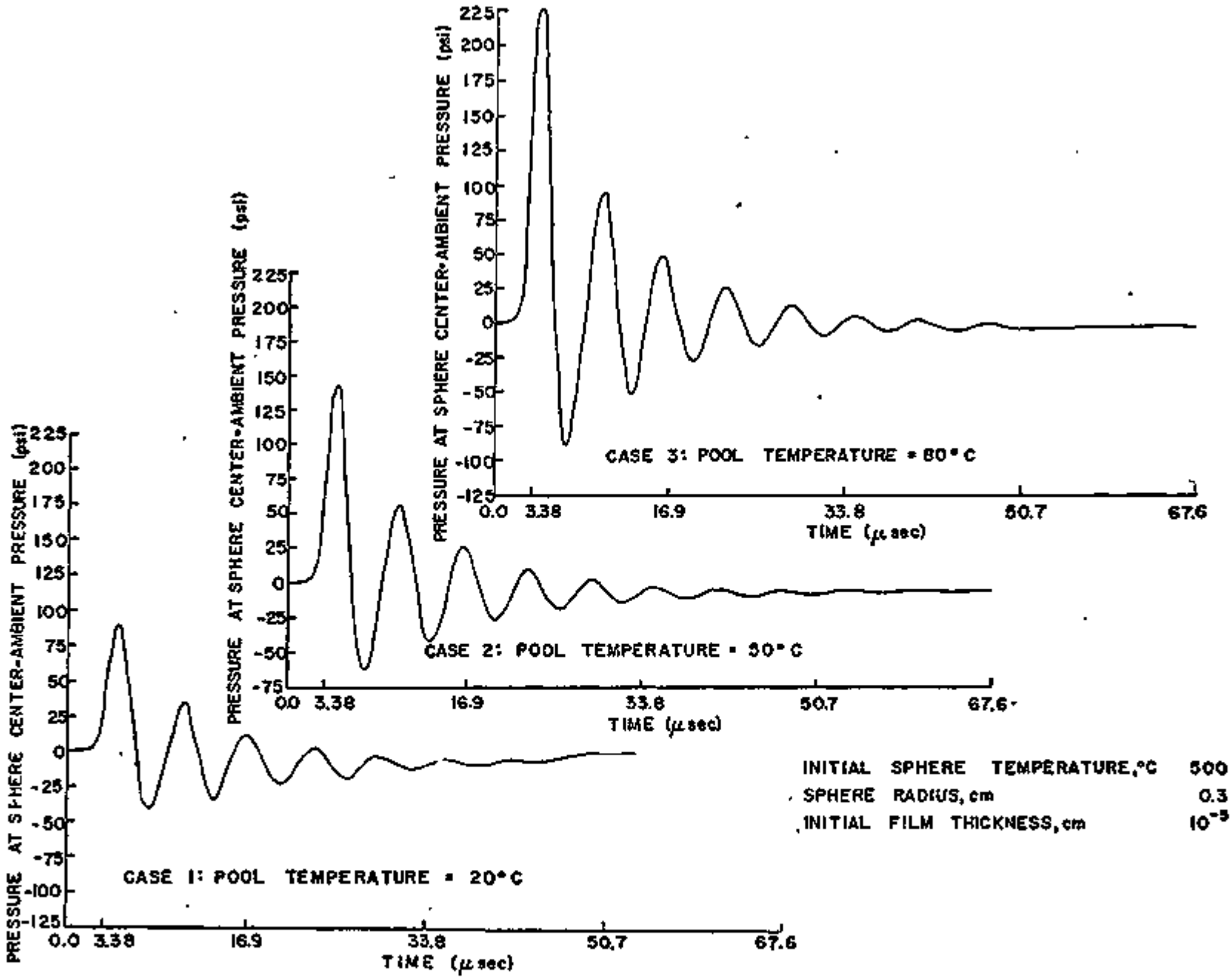

Figure 7. Effect of Pool Temperature on Interior Sphere Pressure History.

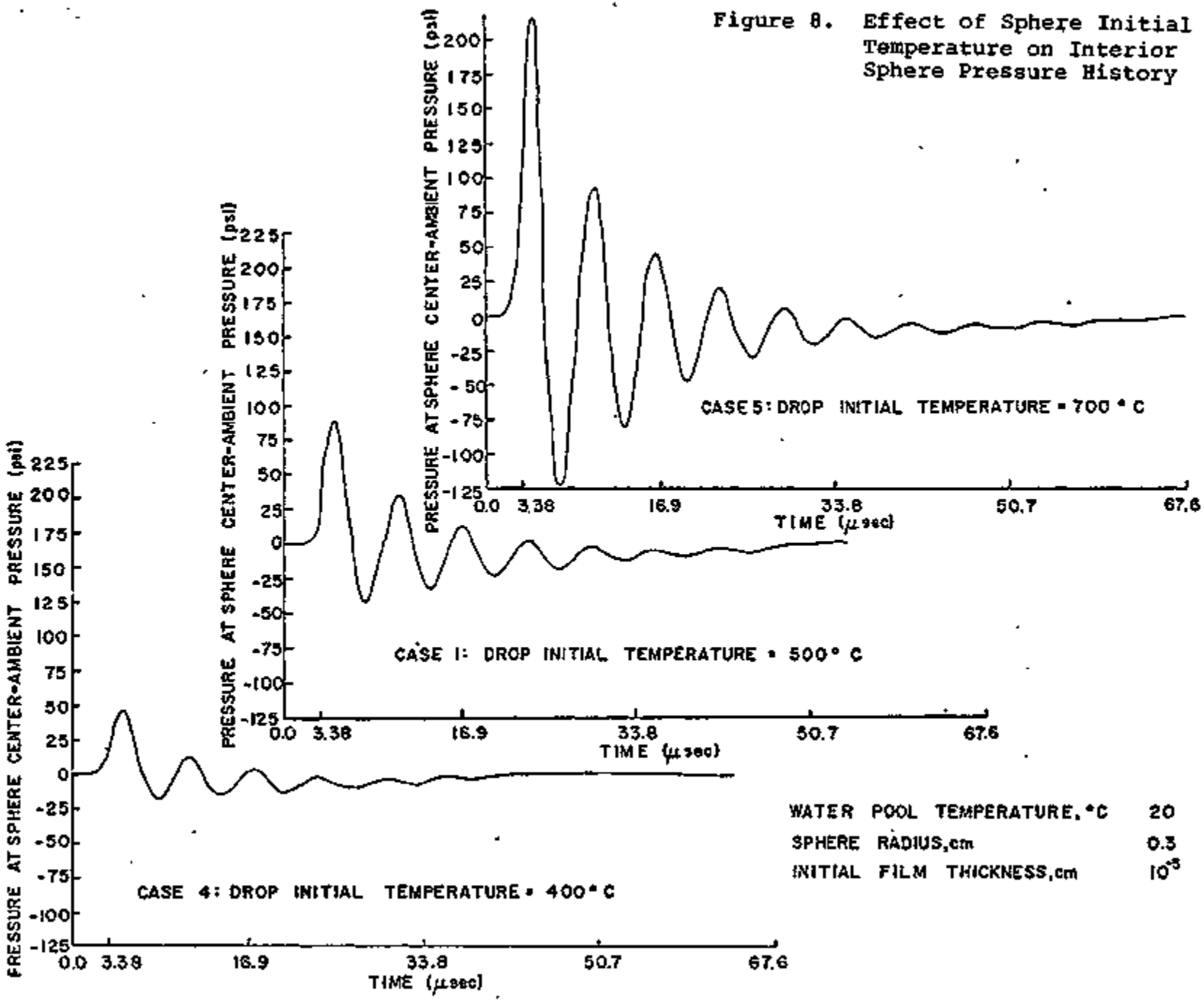

Figure 8. Effect of Sphere Initial Temperature on Interior Sphere Pressure History

Figure 9. Effect of Sphere Radius on Interior Sphere Pressure History

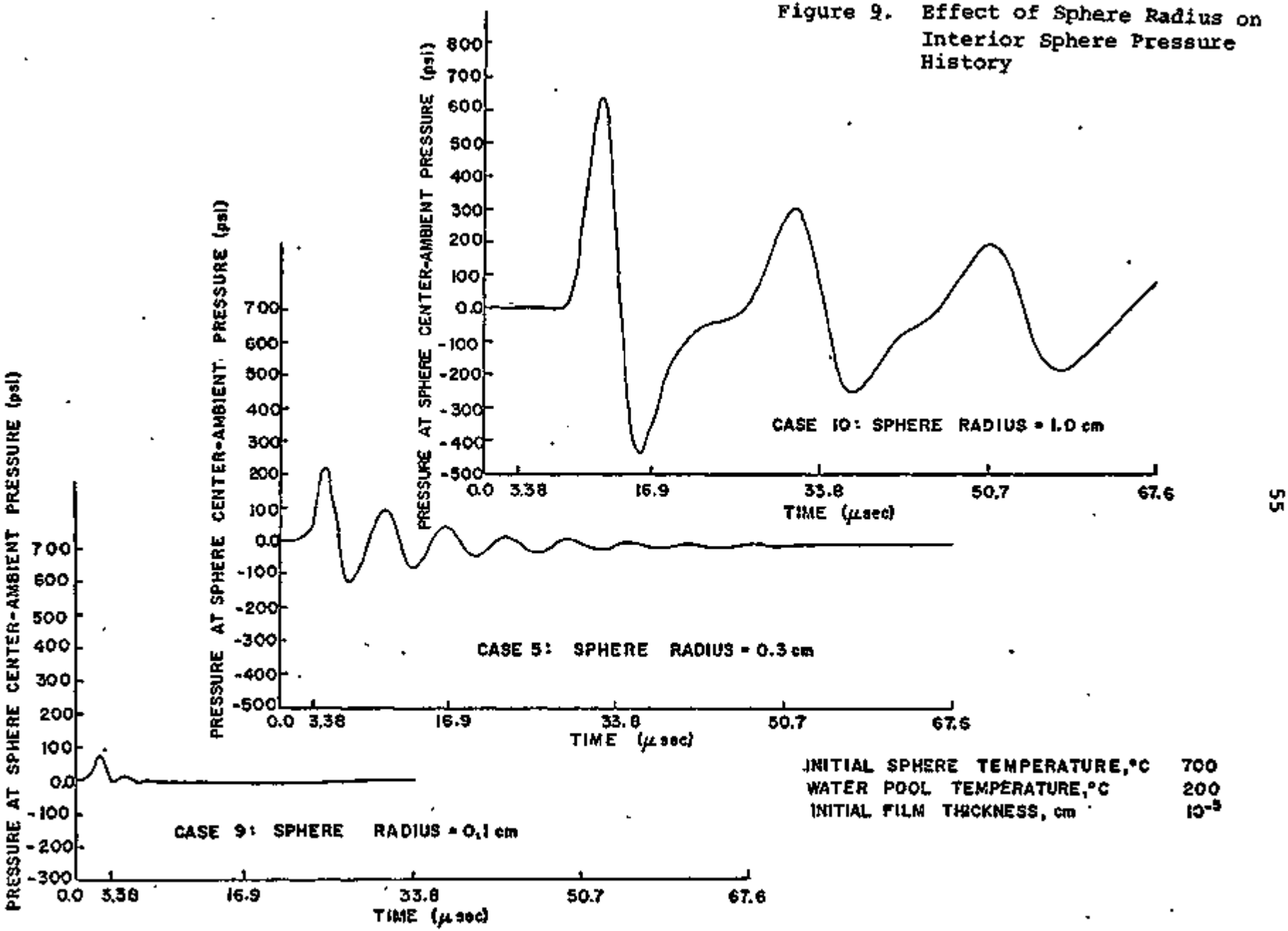

Figure 10. Postulated Composite Interior Sphere Pressure History for Typical Case

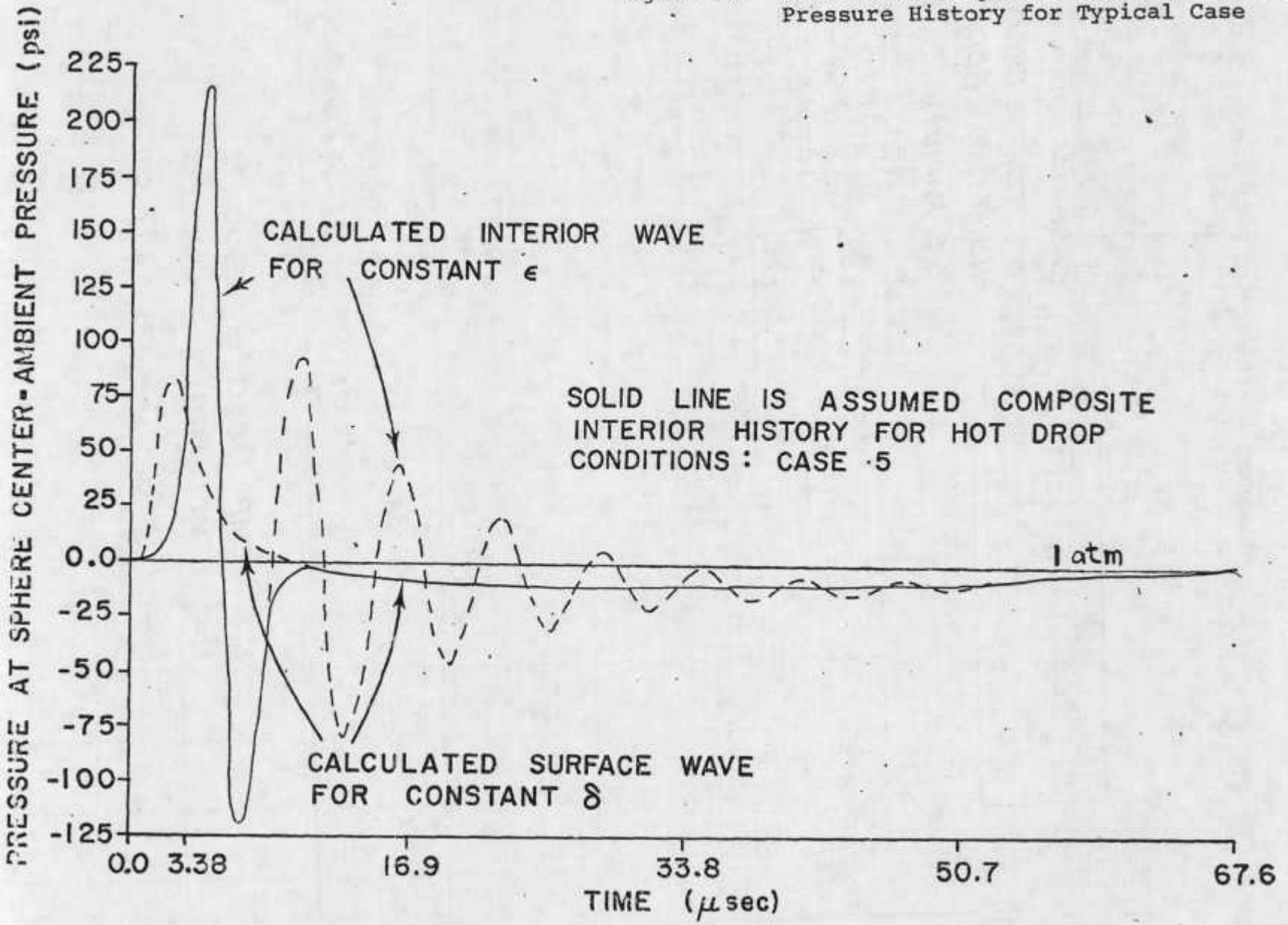

THIS PAGE

WAS INTENTIONALLY

LEFT BLANK

APPENDIX I

FRAGMENTATION ENERGY CALCULATION

Hot Material: stainless steel, $T_{hot} = 2200^{\circ}C$

$\sigma = 1200$ dyne/cm, $R = .35$ cm

Coolant: sodium, $T_{cool} = 85^{\circ}C$

Work done by growing film: From Fig. 4.14 & Fig. 4.15)

p = pressure

t = film thickness

Δv = change in volume of film = $4\pi R^2 t$

Time Interval (10^{-6} sec)	p(dyne/cm^2)	t(cm)	Δv(cm^3)	pΔv(erg)
1.0 - 1.3	3.1×10^6	0	0	0
1.3 - 1.6	2.9×10^6	$.02 \times 10^{-4}$	3.1×10^{-6}	9.0
1.6 - 2.0	2.7×10^6	$.025 \times 10^{-4}$	3.8×10^{-6}	10.3
2.0 - 2.4	2.4×10^6	$.039 \times 10^{-4}$	6.0×10^{-6}	14.4
2.4 - 2.9	2.2×10^6	$.041 \times 10^{-4}$	6.3×10^{-6}	13.4
2.9 - 3.7	1.9×10^6	$.115 \times 10^{-4}$	17.7×10^{-6}	33.6
3.7 - 4.6	1.7×10^6	$.13 \times 10^{-4}$	20.0×10^{-6}	34.0
4.6 - 6.0	1.5×10^6	$.27 \times 10^{-4}$	41.6×10^{-6}	62.4
6.0 - 8.0	1.3×10^6	$.56 \times 10^{-4}$	86.0×10^{-6}	111.8
8.0 - 11.3	1.2×10^6	1.0×10^{-4}	154×10^{-6}	184.8
11.3 - 19	1.1×10^6	2.0×10^{-4}	339×10^{-6}	372.9
19 - 29	1.0×10^6	3.0×10^{-4}	462×10^{-6}	462.9
29 - 53	$.9 \times 10^6$	7.0×10^{-4}	1078×10^{-6}	970.2
53 - 100	$.9 \times 10^6$	5.5×10^{-4}	855×10^{-6}	769.5

APPENDIX II

PARTITION OF ENERGY BETWEEN SS & Na [42]

$$E_{tr} = 2\pi R_{jet}^2 \tau_{ST} \frac{P_{ST}(p_{ST} - p_\infty)}{\rho_f} \left[\frac{1}{C_o} + \frac{\tau_{ST}}{R_{jet}}\right]$$

where ρ_f, density, and C_o, speed of sound, are properties of the medium

R_{jet}, τ_{ST}, P_{ST}, and p_∞ are not functions of the transmitting medium

$$\text{Estimate of } \frac{\text{ENERGY into SS}}{\text{ENERGY into Na}} = \frac{(E_{tr})_{SS}}{(E_{tr})_{Na}} = \frac{\rho_{Na}}{\rho_{SS}},$$

if

$$\frac{\tau_{ST}}{R_{jet}} >> \frac{1}{C_o} \quad \text{and} \quad (C_o)_{Na} = (C_o)_{SS}$$

$$3050 \text{ erg} = \text{ENERGY into SS} + \text{ENERGY into Na}$$

$$= \text{ENERGY into SS } \left(1 + \frac{\rho_{SS}}{\rho_{Na}}\right)$$

$$E_f = \text{ENERGY into SS} = \frac{3050 \text{ erg}}{\left(1 + \frac{\rho_{SS}}{\rho_{Na}}\right)}$$

APPENDIX III

ENERGY REQUIRED FOR FRAGMENTATION

R = initial radius of hot material

R_f = final radius of hot material

A = initial surface area of hot material

A_f = final surface area of hot material

V = volume

$$E_f = (A_f - A)\sigma$$

$$A_f = \frac{E_f}{\sigma} + A$$

$$\frac{A_f}{V} = \frac{E_f}{\sigma V} + \frac{A}{V}$$

but

$$\frac{A_f}{V} = \frac{3}{R_f}, \quad \frac{A}{V} = \frac{3}{R}, \quad \text{and} \quad V = \frac{4}{3}\pi R^3$$

$$\frac{1}{R_f} = \frac{E_f}{4\,R^3_f} + \frac{1}{R}$$

$$R_f = \left[\frac{E_f}{4\pi R^3 \sigma_f} + \frac{1}{R}\right]^{-1}$$

APPENDIX IV

Experimental Data [43]

Sodium Temp (°C)	SS Temp (°C)	Radius (cm)	Mean Diam of Residual (μm)	Mean Diam of Ejected Residual (μm)
200	1800	.78	4400	2200
200	2100	.87	960	--
400	1850	.97	790	710
405	2300	.83	620	620
595	1850	.81	840	820
600	2250	.66	800	920

APPENDIX V

Energy transmitted into sphere or coolant

$$E = \int_0^T \left[\int_s \frac{dE}{dT}\, dA \right] dT \tag{1}$$

$$\frac{dE}{dT} = p(a)\ u_r(a), \text{ pressure } * \text{ velocity} \tag{2}$$

if p and u_r are constant over surface, s, then

$$E(t) = 2\pi \int_0^T a^2(t)\ p(a)\ u_r(a)\ dt \tag{3}$$

in the case of the hot sphere, a(t) ≈ constant

$$E(T) = 2\pi\ a^2 \int_0^T p(a)\ u_r(a)\ dt \tag{4}$$

so we need $u_r(a)$.

Using conservation of momentum (one dimensional, radial)

$$\rho\ \frac{\partial u_r}{\partial t} = -\ \frac{dp}{dr} \tag{5}$$

Notation: $u_r(w) = -\ \frac{dp_w}{dr}$

Taking the Fourier transform (F.T.) of (5)

$$\rho(iw)\ u_w = -\ \frac{dp_w}{dr} \tag{6}$$

$$u_r = \int_{-\infty}^{\infty} u_w\ e^{-iwt}\ dw \tag{7}$$

$$u_w = \frac{i\sqrt{2}}{\rho w}\ \frac{dp_w}{dr} \tag{8}$$

From C.E.W. Thesis (45)

$$p_w(r) = \frac{a}{r} \frac{\sin kr}{\sin ka} p_w(a) \tag{9}$$

$$\frac{dp_w}{dr} = \frac{p_w(a)}{\sin ka}\left(\frac{-a}{r^2} \sin kr + \frac{ka}{r} \cos kr\right) \tag{10}$$

$$= p_w(a) \frac{a}{r} \frac{\sin kr}{\sin ka} \left(h \cot kr - \frac{1}{r}\right) \tag{11}$$

$$\frac{dp_w}{dr} = p_w(a)\frac{ka}{r} \frac{\sin kr}{\sin ka} \left(\cot kr - \frac{1}{kr}\right) \tag{12}$$

at r = a

$$\frac{dp_w}{dr} = \underset{r=a}{\quad} = p_w(a)\ k \left(\cot ka - \frac{1}{ka}\right) \tag{13}$$

Equation (13) is slightly different from C.E.W. thesis using (13) in (8) →

$$u_w(a) = \frac{i\sqrt{2}}{\rho} p_w(a)/c \left(\cot ka - \frac{1}{ka}\right) \tag{14}$$

$$u_w(a) = \frac{i\sqrt{2}}{\rho c} \left(\cot ka - \frac{1}{ka}\right) p_w(a) \tag{15}$$

where $\rho c = \sqrt{\rho/K_T}$, characteristic acoustic impedance p. 259 Morse and K_T = isothermal compressibility.

so

$$u_r = \int_{\infty}^{\infty} \frac{i\sqrt{2}}{\rho c} \left(\cot ka - \frac{1}{ka}\right) p_w(a)\ dw \tag{16}$$

Use Eqs. (16) and (3) to get the work E.

APPENDIX VI

REFLECTION AND TRANSMISSION AT A BOUNDARY

In this part plane boundaries and plane waves are used in order to avoid working out the spherical case. The spherical case is probably not too much harder.

From page 711 MIT (Morse and Ingard) [44]

R (reflection coefficient) =

$$(\rho_2 c_2 - \rho_1 c_1)/(\rho_2 c_2 + \rho_1 c_1) \quad (1)$$

T (transmission coefficient) = 1 + R (2)

$$\epsilon \equiv \frac{\rho_1 c_{1g}}{\rho_2 c_{21}} << 1; \text{ for gas-cold liquid interface} \quad (3)$$

$$R = \frac{1-\epsilon}{1+\epsilon} = (1-\epsilon)(1-\epsilon)(1+\epsilon) = 1-2\epsilon \quad (3)$$

$$R = 1-2\,\rho_1 c_1/\rho_2 c_2 \quad (4)$$

$$T = 2-2\,\rho_1 c_1/\rho_2 c_2 \quad (5)$$

The transmitted pressure wave is equal to twice the reflected wave but is approximately equal to the reflected plus incident wave. For the hot liquid-gas interface

$$\rho_1 c_{1\ell} >> 2 c_{2g}; \quad \epsilon \equiv \frac{\rho 2 c_2}{\rho_1 c_1} << 1 \quad (6)$$

$$R = \epsilon-1/(\epsilon+1) = 1 + 2\epsilon \quad (7)$$

$$T = 1 + R = 2\,\rho_2 c_2/\rho_1 c_1 \approx 0 \quad (8)$$

so in this case there is no transmitted wave.

The formula for the energy density is used

$$W = p^2/\rho c^2 \qquad \text{p. 258 (MIT) [44]} \qquad (9)$$

At the cold liquid-vapor interface

$$\frac{W \text{ (transmitted to cold liquid)}}{W \text{ (vapor film)}} = \frac{\rho c^2 \text{ (gas)}}{\rho c^2 \text{ (liquid)}} \qquad 0$$

since p (transmitted) = p (incident) + p (reflected)

At the hot liquid-vapor interface

$$\frac{W \text{ (transmitted to gas)}}{W \text{ (hot liquid)}} = \frac{\rho c^2 \text{ (hot liquid)}}{\rho c^2 \text{ (gas)}} \times \left(\frac{2\rho c \text{ (gas)}}{\rho c \text{ (hot liquid)}}\right)^2$$

$$= 4 \frac{\rho \text{ (gas)}}{\rho \text{ (hot liquid)}} \cong 0$$